2023-07-01

Time-dependent water wave scattering by a marine structure consisting of an array of compound porous cylinders

Bora, SN

10.1063/5.0147809
Physics of Fluids
American Institute of Physics

Title:

Time-dependent water wave scattering by a marine structure consisting of an array of compound porous cylinders

Journal:

Physics of Fluids

Author names and affiliations:

Swaroop Nandan Bora,[1] Santu Das,[2] Michael H. Meylan,[3] Sunanda Saha,[4, 5, a)] and Siming Zheng[6]

1) Department of Mathematics, Indian Institute of Technology Guwahati, Guwahati, India

2) Mathematical and Computational Sciences (Physical Sciences Division), Institute of Advanced Study in Science and Technology, Guwahati, India

3) School of Information and Physical Sciences, The University of Newcastle, Newcastle, Australia

4) Centre for Clean Environment, Vellore Institute of Technology, Vellore - 632014, India

5) Department of Mathematics, School of Advanced Sciences, Vellore Institute of Technology, Vellore - 632014, India

6) School of Engineering, Computing and Mathematics, University of Plymouth, Plymouth, United Kingdom

a) Corresponding author: sunanda.saha@vit.ac.in

accepted 12 June 2023

Time-dependent water wave scattering by a marine structure consisting of an array of compound porous cylinders

Swaroop Nandan Bora,[1] Santu Das,[2] Michael H. Meylan,[3] Sunanda Saha,[4,5,a)] and Siming Zheng[6]

[1)]Department of Mathematics, Indian Institute of Technology Guwahati, Guwahati, India

[2)]Mathematical and Computational Sciences (Physical Sciences Division), Institute of Advanced Study in Science and Technology, Guwahati, India

[3)]School of Information and Physical Sciences, The University of Newcastle, Newcastle, Australia

[4)]Centre for Clean Environment, Vellore Institute of Technology, Vellore - 632014, India

[5)]Department of Mathematics, School of Advanced Sciences, Vellore Institute of Technology, Vellore - 632014, India

[6)]School of Engineering, Computing and Mathematics, University of Plymouth, Plymouth, United Kingdom

(Dated: 22 May 2023)

Under the assumption of linear wave theory, a semi-analytical model is developed to address the time-dependent water wave scattering problem involving a marine structure consisting of several circular rigid vertical cylinders each of which is surrounded by a thin cylindrical porous wall with a water region between the inner cylinder and the wall. The problem is tackled by applying the eigenfunction expansion approach. The energy dissipation relation is also derived for the system of compound cylinders. The principal focus of this work lies in locating the optimum geometrical con gurations for which the wave forces acting on the structure are minimal along a given wave direction in the frequency domain. Subsequently, the time-dependent response of the structure under the impact of a Gaussian wave pulse is examined. The wavenumber at which the force acting on the inner cylinder is at its maximum is obtained for a given value of the porous-e ect parameter. Moreover, the value of that corresponding wavenumber decreases as the magnitude of the porous-e ect parameter increases. The model is also carefully validated numerically against results available in the existing literature.

[a)] Corresponding author:sunanda.saha@vit.ac.in

I. INTRODUCTION

The engineering design of many marine structures consists of an array of cylinders of circular form. Applications of such structures include columns of tension-leg platforms, wave-power stations, ocean bridges, semi-submersibles, and floating airports. Utilization of these structures, in principle, aids in enhancing and reducing the wave forces acting on the structures. For ocean platforms employed by the oil and gas industry, reducing environmental loading is the key to safety, whereas wave energy converters are constructed to use the highest proportion of the energy that is available. It is obvious that the amount of energy converted into mechanical power is maximised in direct proportion to the amount of induced wave forces.

As a result of multiple wave scattering, strong hydrodynamic interactions between the cylinders occur. These interactions may directly affect the exciting forces acting on it, and which in turn affect the performance metric of the cylinders. These aforementioned interactions depend strongly on the arrangement of the cylinders, distance between the centers of the cylinders and also the wave characteristics of the incident wave. The aim for maximising and minimising the exciting forces acting on these marine structures can be obtained by fine tuning those parameters and optimizing them accordingly. Hence, investigating the wave impact on these structures and obtaining suitable layout configuration of multiple cylinders is of paramount importance for the research community.

Extensive research work has already been carried forward in these directions and the theory is well established for a specific pre-defined configuration. Considering the array of two and three horizontal/vertical cylinders, the wave diffraction and radiation problem was first reported in the literature during the 20th century by Spring and Monkmeyer[1] through an eigenfunction expansion approach. Using a "plane-wave" approximation that enables the multiple-scattering problem to be penned as a matrix equation, Simon[2] examined the multiple scattering of evenly-spaced linear arrays of identical axisymmetric devices. Employing a large-spacing approximation and substituting plane waves for scattered divergent waves, McIver and Evans[3] established an approximation technique for the estimation of wave forces on groups of fixed vertical cylinders. Kagemoto and Yue[4] described a general approach for computing the wave hydrodynamics of a multi-member structure based on the diffraction characteristics of individual members. Their method can be used for different types, sizes,

and arrangements of any structure, with the exception of those with crossing vertical projections. By streamlining the expression for the velocity potential near a specific cylinder, Linton and Evans[5] improved the method adopted by Spring and Monkmeyer[1]. This has led to simple formulas for the first- and mean second-order forces acting on the body as well as to an effective technique for calculating free-surface amplitudes.

As can be understood from the discussed literature above, numerous methods have been developed so far for solving the hydrodynamic problem of multiple impermeable cylinders with arrays. It is an important requirement to safeguard those structures, thereby increasing their longevity. It is well established in the literature that a porous wall around a vertical cylinder decreases the wave energy impact on the enclosed cylinder[6{12]. All these works, except for the last one, considered the porous wall to be cylindrical in shape, whereas the last one considered the porous wall to be of arbitrary shape and investigated the problem by using the scaled boundary finite element method. A porosity range that would minimize the wave impact was suggested through an experiment on the discussed set-up and reported in the work of Vijayalakshmi et al.[13]. In another direction, work has been carried out by enclosing two porous walls around a vertical cylinder to study the impact of a solitary wave on the cylinder[14]. Earlier investigations provide the impetus to consider the diffraction problem in the presence of multiple compound cylinders. Hence, enclosing these vertical cylinders with porous material may safeguard the cylinder. Williams and Li[15] theoretically examined the hydrodynamic forces and run-up on an array of bottom-mounted, surface-piercing circular cylinders, each of which had a porous sidewall. The study was based on the method proposed by Linton and Evans[5]. The effects of the porous cover on sound attenuation by periodic arrays of cylinders was investigated by Umnova et al.[16]. In order to provide the semi-analytical solution of the interaction between regular waves and an array of dual porous circular cylinders, Sankarbabu et al.[17] extended the work of Williams and Li. A three-dimensional numerical analysis method was developed by Park et al.[18] to analyze the wave forces acting on the array of dual cylindrical cylinders with partial porous area. It is suggested that the annular region between the porous wall and the vertical cylinder can be utilized for extensive aquaculture farms[19], which will likely cut down expenditure to a reasonable extent on both public and private fronts.

When we include numerous resonant frequencies and try to understand the impact through time domain analysis, the study becomes more challenging due to various fac-

tors, but it allows us to realize the long-term influence of multiple wave scattering on the structure, which is not achievable through a frequency domain solution. Such investigations have gained more and more attention recently, and provide us with the impetus to take up the present work. Time-dependent responses owing to a moving load on a flexible floating plate and a visco-elastic plate are shown in earlier works[20,21]. The time domain solution can be expressed as the sum of decaying modes obtained from the frequency domain by using the generalized eigenfunction expansion method. Using the same technique, the solution is visualized for a floating elastic plate[22–24]; an array of cylinders[25]; multiple flexible fishing cage system[26]; compound porous cylinder in which a porous lid covered the annular region of the structure[27]. Although a sizeable number of studies have been accomplished that demonstrate time domain simulation for floating plates, to the best of the authors' knowledge, the scope for time-dependent analysis for wave scattering by multiple compound porous cylinders remains untouched.

Based on the necessity and to achieve the goal mentioned above, in this paper, we consider a model consisting of N compound porous cylinders arranged in a block form that resembles a specific type of marine structure as suggested by Sankarbabu et al.[17]. First, by considering one single frequency wave, the analytical solution will be presented in the frequency domain. The energy dissipation relation will be derived by deploying the energy identity relations which has not been performed in the earlier works. After validating the numerical results with the existing literature on vertical cylinders, the influence of the spacing of the compound cylinders and values of the complex porous-effect parameter on wave forces and wave run-up will be numerically analyzed for configurations of four, five and nine compound structures. The specific values of the wavenumber at a frequency having a substantial impact on the wave forces will also be identified. Then using those wavenumbers, the time-dependent solution will be built from the frequency domain analysis due to the presence of a Gaussian impulse. The time domain simulations will help visualize the water wave scattering problem and comprehend the compound cylinder's long-term behaviour and the impact of the force term. Understanding of the scattering problem of the arrays of compound structures through time-domain simulation and derivation of the energy dissipation relation in the frequency domain may be considered the novelty of the present work. It may be noted that the present physical model may look similar to the one in Sankarbabu et al.[17], but the objectives are quite different.

The flow of this paper is structured as follows. The mathematical model of the wave scattering problem is described in Section II. The theoretical solutions for spatial velocity potentials are presented in the frequency domain in Section III. This section provides the techniques for calculating the potential function (III.A), wave power dissipation (III.B) and wave forces (III.C). Following validation, the model is used to conduct a multi-parameter analysis; the findings are presented in III.D. Section IV details the time-dependent solutions to the problem. The paper ends with a brief conclusion in Section V.

II. MATHEMATICAL FORMULATION

In this model, N number of bottom-mounted compound cylinders with porous boundaries are conceptually deployed as an array in water of finite depth. Each compound cylinder contains a water region between the vertical cylinder and the porous wall (Fig. 1). Let a_j and b_j be the respective radius of the inner (solid) and outer cylinder (thin porous wall) of the j-th compound cylinder, where $j = 1; 2; \dots; N$. The Cartesian coordinate system

FIG. 1. Schematic presentation of an array of bottom-mounted compound porous cylinders: (a) bird's eye view, (b) top view

$(x; y; z)$ originates on the mean free surface, with z pointing upwards, whereas $z = 0$ is taken as the mean free surface and $z = -H$ is the flat bottom. A monochromatic incident wave train of small amplitude A and frequency ω, travelling in the direction β relative to the positive Ox axis, is assumed to strike the structure. Further, we consider the origin of each compound cylinder as the center of the local coordinate systems given by $O_j(r_j; \theta_j)$ as shown in Fig. 1(b). In terms of the Cartesian coordinate system $Oxyz$, the origin of the

j-th cylinder can be expressed as (x_j, y_j). The entire fluid domain is then divided into $N+1$ sub-domains: $\Omega_j = \{(r_j, \theta_j, z) \mid a_j \quad r_j \quad b_j, 0 \quad \theta_j \quad 2\pi, \quad H < z < 0\}$ for $j = 1, 2, \ldots, N$; and $\Omega_{N+1} = R^3 \setminus (\Omega_1 \cup \Omega_2 \cup \quad \cup \Omega_N)$. Within the framework of the potential flow theory, the flow is assumed to be inviscid, incompressible and irrotational. Thus, the flow field can be described by a complex velocity potential Φ satisfying Laplace's equation:

$$\nabla^2 \Phi(x, y, z, t) = 0, \tag{1}$$

where t represents time.

The free surface and bottom boundary conditions are as follows:

$$\frac{\partial \Phi}{\partial z} + \frac{1}{g}\frac{\partial^2 \Phi}{\partial t^2} = 0, \quad \text{on} \quad z = 0, \quad r_j > a_j, \tag{2}$$

$$\frac{\partial \Phi}{\partial z} = 0, \quad \text{on} \quad z = \quad H, \tag{3}$$

where g represents the acceleration due to gravity.

The matching conditions on the porous wall ($r_j = b_j$) and on the impermeable cylinder ($r_j = a_j$) for each compound cylinder can be expressed as

$$\frac{\partial \Phi}{\partial r_j}_{r_j = b_j^+} = \frac{\partial \Phi}{\partial r_j}_{r_j = b_j} = ikG_j \quad \Phi_{r_j = b_j} \qquad \Phi_{r_j = b_j^+}, \quad \text{on} \quad r_j = b_j, \tag{4}$$

$$\frac{\partial \Phi}{\partial r_j} = 0, \quad \text{on} \quad r_j = a_j, \tag{5}$$

where G_j is the linearized porous-effect parameter, as in Yu[28], for the porous wall of the j-th compound cylinder with $j = 1, 2, \ldots, N$ and k is the wavenumber of the considered wave train. Let the origin of the global cylindrical coordinate system be denoted by $O_0(r_0, \theta_0, z)$, which coincides with the origin of the Cartesian coordinate system. Then the Sommerfeld radiation condition at the far-field is[29]

$$\lim_{r_0 \to \infty} \sqrt{kr_0}\left(\frac{\partial \Phi}{\partial r_0} \quad ik\Phi\right) = 0. \tag{6}$$

In the subsequent sections, we look at the problem from two perspectives: frequency domain analysis and then an extension to time domain forcing.

III. FREQUENCY DOMAIN PROBLEM

A. Theoretical solution to velocity potentials

The time factor can be separated from each potential by considering the time-harmonic nature of the incident wave. Also, the z-dependency can be separated by using the separation of variable technique in Eq. (1) and boundary conditions (2) and (3), and subsequently, the velocity potential in the j-th domain can be written as

$$\Phi(x, y, z, t) = \frac{-\mathrm{i}Ag}{\omega}\psi(z)\phi(x, y)e^{\ \mathrm{i}\omega t}, \tag{7}$$

with $\psi(z) = \dfrac{\cosh k(z + H)}{\cosh kH}$; i the imaginary quantity given by $\mathrm{i} = \sqrt{-1}$ and k the wavenumber which satisfies the dispersion relation $\alpha = k\tanh(kH)$ where $\alpha = \omega^2/g$.

The wave elevation on the free surface in the frequency domain can also be computed by using linearized Bernoulli's equation:

$$\eta(x, y, t) = A\tilde{\eta}(x, y)\ \ ^{\mathrm{i}\omega t}, \tag{8}$$

with $\tilde{\eta}(x, y) = \phi(x, y)$.

The two-dimensional components of the velocity potential in the exterior domain may be expressed as

$$\phi(r_j, \theta_j) = \phi_{\mathrm{inc}}(r_j, \theta_j) + \sum_{m=1}^{\infty}\sum_{j=1}^{N} A_m^j H_m(kr_j)e^{\mathrm{i}m\theta_j} \quad \text{for} \quad r_j \in \Omega_{N+1}\,, \tag{9}$$

where ϕ_{inc} represents the incident wave potential. The second term on the right hand side denotes the components contributed by the waves scattered from N compound cylinders; A_m^j are the unknown coefficients to be determined; $H_m(.)$ denotes the Hankel function of first kind of order m. The velocity potential in the interior region of each compound cylinder may be expressed as

$$\phi(r_j, \theta_j) = \sum_{m=1}^{\infty} B_m^j U_m(kr_j)e^{\mathrm{i}m\theta_j}\,, \quad \text{for} \quad j = 1, 2, \ldots, N, \quad r_j \in \Omega_j, \tag{10}$$

where B_m^j are coefficients representing the amplitude of the waves inside the annular region Ω_j and

$$U_m(kr_j) = J_m(kr_j)H_m'(ka_j) - J_m'(ka_j)H_m(kr_j), \tag{11}$$

with $J_m(.)$ as the Bessel function of first kind of order m. Now the plane incident wave can be written as

$$\phi_{\text{inc}}(r_j,\theta_j) = T_j \sum_{m=-\infty}^{\infty} J_m(kr_j) e^{\mathrm{i}m(\pi/2-\theta_j+\beta)}, \tag{12}$$

where

$$T_j = e^{\mathrm{i}k(x_j\cos\beta + y_j\sin\beta)}. \tag{13}$$

Let the p-th compound cylinder be the fixed one and the j-th compound cylinder be an arbitrary one whose coordinate system is required to be expressed in terms of the coordinates of the p-th compound cylinder. Using Graf's addition theorem[30], Eq. (9) can be rewritten as

$$\begin{aligned}\phi(r_p,\theta_p) = \sum_{m=-\infty}^{\infty} \Bigg[& T_p\, J_m(kr_p) e^{\mathrm{i}m(\pi/2-\theta_p+\beta)} + A_m^p H_m(kr_p) e^{\mathrm{i}m\theta_p} \\ & + \left(\sum_{\substack{j=1,\\ j\neq p}}^{N} \sum_{s=-\infty}^{\infty} A_m^j H_{s-m}(kR_{jp}) e^{\mathrm{i}(s-m)\alpha_{jp}} \right) J_m(kr_p) e^{\mathrm{i}m\theta_p} \Bigg], \quad \text{for} \quad b_p \le r_p \le R_{jp}, \end{aligned} \tag{14}$$

where (R_{jp},α_{jp}) are the polar coordinates of the mean center position of the j-th compound cylinder in the local coordinates of the p-th compound cylinder. Using the boundary condition (4) at $r_p = b_p$ on $\phi(r_p,\theta_p)$ given by Eqs. (10) and (14) and subsequently, applying the orthogonality of the trigonometric functions of θ_p, we get the following two equations for each m:

$$\begin{aligned} A_m^p H_m'(kb_p) + \left(\sum_{\substack{j=1,\\ j\neq p}}^{N} \sum_{s=-\infty}^{\infty} A_s^j H_{s-m}(kR_{jp}) e^{\mathrm{i}(s-m)\alpha_{jp}} \right) J_m'(kb_p) - B_m^p U_m'(kb_p) = \\ -T_p e^{\mathrm{i}m(\pi/2-\beta)} J_m'(kb_p), \end{aligned} \tag{15}$$

$$\begin{aligned} \mathrm{i}G_p \left\{ A_m^p H_m(kb_p) + \left(\sum_{\substack{j=1,\\ j\neq p}}^{N} \sum_{s=-\infty}^{\infty} A_s^j H_{s-m}(kR_{jp}) e^{\mathrm{i}(s-m)\alpha_{jp}} \right) J_m(kb_p) \right\} + B_m^p \gamma_{mp} = \\ -\mathrm{i}G_p T_p e^{\mathrm{i}m(\pi/2-\beta)} J_m(kb_p), \end{aligned} \tag{16}$$

with $\gamma_{mp} = U_m'(kb_p) - \mathrm{i}G_n U_m(kb_p)$, and $'$ representing the differentiation with respect to r_p. Now, multiplying Eq. (15) by γ_{mp} and Eq. (16) by $U_m'(kb_p)$ and adding them, we get an infinite system of equations for the unknown coefficients A_m^p:

$$A_m^p \delta(m,p) + \left(\sum_{\substack{j=1,\\ j\neq p}}^{N} \sum_{s=-\infty}^{\infty} A_s^j H_{s-m}(kR_{jp}) e^{\mathrm{i}(s-m)\alpha_{jp}} \right) = -T_p e^{\mathrm{i}m(\pi/2-\beta)}, \tag{17}$$

with $\delta(m,p) = \dfrac{\pi k b_p H'_m(kb_p)U'_m(kb_p) + 2G_p H'_m(ka_p)}{\pi k b_p J'_m(kb_p)U'_m(kb_p) + 2G_p J'_m(ka_p)}$. Obtaining the values of A_m^p from this equation and substituting in Eq. (15), we can get the values of unknown coefficients B_m^p as

$$B_m^p = I_m^p \frac{J'_m(kb_p)}{U'_m(kb_p)} - A_m^p \frac{H'_m(kb_p)}{U'_m(kb_p)} - \left(\sum_{\substack{j=1,\\ j\neq p}}^{N} \sum_{s=-\infty}^{\infty} A_s^j H_{s-m}(kR_{jp}) e^{\mathrm{i}(s-m)\alpha_{jp}} \right) \frac{J'_m(kb_p)}{U'_m(kb_p)}. \quad (18)$$

Using Eq. (17), and substituting the value of $\delta(m,p)$, we get a simplified form of B_m^p given by

$$B_m^p = \frac{-2G_p A_m^p}{\pi k b_p J'_m(kb_p)U'_m(kb_p) + 2G_p J'_m(ka_p)}. \quad (19)$$

When $G_p = 0$, we have $B_m^p = 0$ and $\delta(m,p) = \dfrac{H'_m(kb_p)}{J'_m(kb_p)}$ and hence Eq. (17) reduces to

$$\overline{A}_m^p + \left(\sum_{\substack{j=1,\\ j\neq p}}^{N} \sum_{s=-\infty}^{\infty} \overline{A}_s^j Z_s^j H_{s-m}(kR_{jp}) e^{\mathrm{i}(s-m)\alpha_{jp}} \right) = -T_p e^{\mathrm{i}m(\pi/2-\beta)}, \quad (20)$$

where $\overline{A}_s^j = \frac{A_s^j}{Z_s^j}$, with $Z_s^j = \dfrac{J'_m(kb_p)}{H'_m(kb_p)}$, which is exactly the same as in Linton and Evans[5].

In order to evaluate the unknowns A_s^j, the infinite system of equations given by Eq. (17) needs to be truncated to a finite system of $N(2M+1)$ equations with $N(2M+1)$ unknowns. Hence Eq. (17) can be rewritten as

$$A_m^p \delta(m,p) + \left(\sum_{\substack{j=1,\\ j\neq p}}^{N} \sum_{s=-M}^{M} A_s^j H_{s-m}(kR_{jp}) e^{\mathrm{i}(s-m)\alpha_{jp}} \right) = -T_p e^{\mathrm{i}m(\pi/2-\beta)},$$
$$\text{with} \quad p = 1, 2, \ldots, N, \;\; m = -M, \ldots, M. \quad (21)$$

Using Eqs. (17) and (19) in the expressions of the two-dimensional velocity potentials given by Eqs. (10) and (14), the simplified form of those potentials can be written as

$$\phi(r_j, \theta_j) = \sum_{n=-\infty}^{\infty} A_n^j S_n^j(kr_j) e^{\mathrm{i}n\theta_j}, \quad \text{for} \;\; b_j \leq r_j \leq R_{jp} \;\; \forall p, \quad (22)$$

$$\phi(r_j, \theta_j) = \sum_{n=-\infty}^{\infty} A_n^j L_n^j(kr_j) e^{\mathrm{i}n\theta_j} \quad \text{for} \;\; a_j \leq r_j \leq b_j, \quad (23)$$

where $S_n^j(kr_j) = H_n(kr_j) - \delta(n,j) J_n(kr_j)$ and $L_n^j(kr_j) = \dfrac{-2G_j U_n(kr_j)}{\pi k b_j J'_n(kb_j)U'_n(kb_j) + 2G_j J'_n(ka_j)}$.

B. Far- eld scattering amplitudes

Far away from the vicinity of the compound cylinders, the scattered potential represented by the cumulative terms in Eq. (9) can be written as

$$\phi_s = \frac{e^{i(\pi/4+kr_0)}}{\sqrt{2\pi kr_0}} A_s(\theta_0), \quad \text{for } r_0 \to \infty, \tag{24}$$

where $A_s(\theta_0)$ is the scaled version of the far-field coefficient which is given by

$$A_s(\theta_0) = 2\sum_{j=1}^{N}\sum_{n=-\infty}^{\infty} A_n^j e^{-ikR_j\cos(\alpha_j-\theta_0)}(-i)^{n+1}e^{in\theta_0}, \tag{25}$$

where (R_j, α_j) represents the polar coordinates of the mean center position of the j-th compound cylinder from the global cylindrical coordinate system $O_0(r_0, \theta_0, z)$.

C. Wave power dissipation

Now we proceed to compute the energy dissipation by the compound cylinder system. The average power dissipation P_{diss} by N compound cylinders due to the presence of the porous wall can be calculated by

$$P_{\text{diss}} = \sum_{j=1}^{N}\iint_{\partial\Omega_j} \overline{\nabla p \frac{\partial\Phi}{\partial n}} ds, \tag{26}$$

where p denotes the hydrodynamic pressure on the surface of the compound cylinder and is defined by $p = \mathrm{i}\omega\rho\Phi$ with ρ denoting the density of the water. Also, $\partial\Omega_j$ is the union of the porous wall at $r_j = b_j$ and the impermeable wall at $r_j = a_j$. Since $\dfrac{\partial\Phi}{\partial n} = 0$ on $r_j = a_j$, therefore, Eq. (26) can be simplified further, by using Eq. (4), as

$$\begin{aligned} P_{\text{diss}} &= \sum_{j=1}^{N}\iint_{\Omega_j, r_j=b_j}\left[(\Phi_{r_j=b_j} - \Phi_{r_j=b_j^+})\frac{\partial\Phi^*}{\partial r_j} - \left(\Phi_{r_j=b_j} - \Phi_{r_j=b_j^+}\right)^*\frac{\partial\Phi}{\partial r_j}\right] ds \\ &= -\frac{\rho \mathrm{i} A^2\omega g}{4\alpha}\sum_{j=1}^{N} 2\mathrm{i}k\mathrm{Re}(G_j)\int_{-H}^{0}\psi^2(z)dz\int_0^{2\pi}\left|\phi_{r_j=b_j} - \phi_{r_j=b_j^+}\right|^2 d\theta. \end{aligned} \tag{27}$$

This can further be simplified as

$$P_{\text{diss}} = \frac{\rho g A^2}{2}\pi c_g \sum_{j=1}^{N}\mathrm{Re}(G_j)\sum_{n=-\infty}^{\infty}\left|A_n^j\left(S_n^j(kb_j) - L_n^j(kb_j)\right)\right|^2, \tag{28}$$

by using the expressions of the velocity potentials from Eqs. (22)-(23) and $c_g = \frac{\omega}{2k}\left(1 + \frac{2kH}{\sinh 2kH}\right)$[31]. Let P_{inc} be the wave power of the incident wave per unit width of the wavefront and given by

$$P_{\text{inc}} = \frac{\rho g A^2}{2} c_g. \tag{29}$$

Then the energy dissipated by the cylinders can be written in the non-dimensional form as

$$\eta_{\text{diss}} = \frac{P_{\text{diss}}}{P_{\text{inc}}} = \pi \sum_{j=1}^{N} \text{Re}(G_j) \sum_{n=-\infty}^{\infty} \left| A_n^j \left(S_n^j(kb_j) - L_n^j(kb_j) \right) \right|^2. \tag{30}$$

D. Forces

The exciting forces acting on the j-th inner cylinder and its surrounding porous wall can, respectively, be evaluated by integrating the pressure distribution on the compound cylinder and are given by

$$\widetilde{F}_{\text{in}}^j = -\frac{\rho g A a_j}{k} \tanh(kH) \int_0^{2\pi} \phi(a_j, \theta_j) \cos\theta_j \, d\theta_j, \tag{31}$$

$$\widetilde{F}_{\text{out}}^j = -\frac{\rho g A b_j}{k} \tanh(kH) \int_0^{2\pi} \left[\phi(b_j^+, \theta_j) - \phi(b_j^-, \theta_j) \right] \cos\theta_j \, d\theta_j, \tag{32}$$

where $\widetilde{F}_{\text{in}}^j$ represents the force on the j-th inner cylinder and $\widetilde{F}_{\text{out}}^j$ represents the same on its surrounding porous wall.

For simplicity, we consider the same geometrical configuration and property for all the compound cylinders, i.e., $a_j = a$, $b_j = b$, $G_j = G$, $j = 1, 2, \ldots, N$. Then, using the expressions for velocity potentials from Eqns. (22)-(23) and applying the orthogonality of the cosine function, the non-dimensionalized form for both the force terms can be rewritten as

$$f_{\text{in}}^j = \left| L_1^j(ka)(A_1^j - A_{-1}^j) \right|, \tag{33}$$

$$f_{\text{out}}^j = \left| \frac{b}{a} \left(S_1^j(kb) - L_1^j(kb) \right) \left(A_1^j - A_{-1}^j \right) \right|, \tag{34}$$

where $f_{\text{in}}^j = \left| \frac{\widetilde{F}_{\text{in}}^j}{Q} \right|$ and $f_{\text{out}}^j = \left| \frac{\widetilde{F}_{\text{out}}^j}{Q} \right|$ with $Q = \frac{\rho g A a}{k} \tanh(kH)$. Solving the system of equations (17), we get the values of the required unknown coefficients, and by substituting the same in the above equations, we can evaluate the force terms for a given set of parameters.

(a) (b)

FIG. 2. (a) Validation with Teng et al. [32] with M = 6; b=a= 2 and = 0° for single compound cylinder; (b) Validation with Evans and Porter [33] with M = 6; G = 0; b=a= 1 and = 0° for four vertical impermeable cylinders

E. Numerical Results in frequency domain

First, to validate our model, we consider the work of Teng et al.[32] in which they considered a porous wall around a rigid cylinder. The results obtained for the force f_{in} from the present model are shown with continuous lines, and the ones corresponding to Tseng et al.[32] are shown with discrete points in Fig. 2(a). From the figure, it can be inferred that the present numerical results are in good agreement with those of Tseng et al.[32]. We further consider the work of Evans and Porter[33] so as to compare our result with a work with an array of cylinders in which there is no porous wall around each rigid cylinder. In this work, four vertical cylinders are placed on a circle of radius R. To match our model with their work, it is required to consider four cylinders that are located on a circle of radius $R = 2\sqrt{2}a$ such that the center of the j-th cylinder is given by $x_j = R\cos(2\pi j/4)$ and $y_j = R\sin(2\pi j/4)$ with $j = 1, 2, 3$ and 4. As depicted in Fig. 2(b), excellent conformity exists between the results, which validates our model and can be considered suitable for further investigation.

After successful validation, we are now in a position to conduct numerical experiments on the problem. In this direction, we are concerned with the forces on three different arrangements of the compound cylinders as given in Fig. 3. Here, in Fig. 3(a), four compound cylinders are placed on the square of length $2h$ and centered at $(0, 0)$. Then, with the same

FIG. 3. Three di erent arrangements of arrays of identical compound cylinders of equal porous-e ect parameter G, with (a) N = 4; (b) N = 5; (c) N = 9

arrangement, one more compound cylinder is added to the configuration at the center, as shown in Fig. 3(b). Finally, in the third set-up, nine compound cylinders are considered as shown in Fig. 3(c), with eight placed on the square of length $2h$ and the other at the center. The parameters involved in numerical computations are kept fixed at $\beta = 0$, $G = 0.1$,

	1st cylinder		2nd cylinder		3rd cylinder		4th cylinder	
	ka = 2:0	ka = 6:0	ka = 2:0	ka = 6:0	ka = 2:0	ka = 6:0	ka = 2:0	ka = 6:0
M = 1	0.2083	0.0529	0.02052	0.0634	0.2052	0.0634	0.2083	0.0529
M = 2	0.2494	0.0420	0.1730	0.0547	0.1730	0.0547	0.2494	0.0420
M = 4	0.2500	0.0333	0.1853	0.0515	0.1853	0.0515	0.2500	0.0333
M = 6	0.2496	0.0303	0.1863	0.0613	0.1863	0.0613	0.2496	0.0303
M = 8	0.2496	0.0310	0.1863	0.0576	0.1863	0.0576	0.2496	0.0310
M = 10	0.2496	0.0307	0.1863	0.0592	0.1863	0.0592	0.2496	0.0307
M = 12	0.2496	0.0309	0.1863	0.0592	0.1863	0.0592	0.2496	0.0309
M = 15	0.2496	0.0309	0.1863	0.0592	0.1863	0.0592	0.2496	0.0309

TABLE I. Variation of f_{in}^{j} for di erent values of M ; with G = 0:1; = 0 b=a= 1:25 and h=a = 3 for four compound cylinders

$b/a = 1.25$ and $h/a = 3.0$ unless otherwise mentioned. The porous-effect parameter value is considered from the work of Vijayalakshmi et al.[13] in which they suggested its range

through an experimental set-up. In Table I, we show the convergence for the force term f_{in}^{j} by considering two different values of wavenumber, viz., $ka = 2$ and $ka = 6$. It can be observed from the table that, for lower values of ka, the solution remains unaltered for $M = 6$ onward, but for higher values of ka, the same occurs from $M = 12$ onward. Hence, for further computation, we keep $M = 15$ unless otherwise mentioned.

Now, before moving on to the study of hydrodynamic forces for the above-discussed set-up, we consider here four compound cylinders arranged as in Fig. 3(a), and the wave power dissipation is shown in Fig. 4. We present the results for different values of G in Fig. 4(a) and b/a in Fig. 4(b). Here, we limit our discussion to real values of G only, although the

(a) (b)

FIG. 4. Wave power dissipation of four compound cylinders: (a) variation of η_{diss} with G for $b/a = 1.2$; (b) variation of η_{diss} with b/a for $G = 0.1$

same analysis can also be performed for complex G. It can be observed from the plots that the dissipation increases with an increase in $G < 1$, whereas for $G > 1$, the dissipation decreases as the value of the porous-effect parameter increases. Also, the dissipation is rapid for $G < 1$. The same analysis has been carried out by Meylan et al.[34]. The behaviour of the scattering amplitude $A_s(\theta_0)$ with a variation of the porous-effect parameter and θ_0 are shown in Figs. 5 and 6. The values of other parameters are kept fixed as discussed before. In Fig. 5, the values of G are considered to be real. It is observed that, for $\theta_0 \in (-15^\circ, 15^\circ)$, the scattering amplitude is high due to the wave reflection within that range since the incident wave angle is 0°. The maximum amplitude is observed for higher

FIG. 5. Scattering amplitude for different values of porous-effect parameter G with $ka = 3$

(a) (b)

FIG. 6. Wave scattering amplitude for (a) $G = \mathrm{Re}(G) + 0.1\mathrm{i}$, (b) $G = 0.1 + \mathrm{Im}(G)\mathrm{i}$ for $ka = 3$

values of the porous-effect parameter as it represents the wave profile in the direction exactly behind the structure. Beyond this range, the scattering amplitude exists only due to the wave transmission, and the damping of the scattering amplitude increases with an increase in the value of the porous-effect parameter. Hence, in Fig. 6(a), the scattering amplitude is plotted against $\mathrm{Re}(G)$ by assuming $\mathrm{Im}(G) = 0.1$ and then, against $\mathrm{Im}(G)$, by assuming $\mathrm{Re}(G) = 0.1$ in Fig. 6(b). It is observed that, with an increase in the value of $\mathrm{Re}(G)$, the

scattering amplitude increases slightly and then converges to a finite value. On the contrary, with an increase in the value of $\mathrm{Im}(G)$, the scattering amplitude increases with a high slope, attains a maximum and then decreases to a finite limit. Hence the porous-effect parameter with a low inertia factor is expected to be more suitable for maintaining a lower scattering amplitude.

With all these analyses, the present theoretical model is well-verified with respect to its efficiency in solving wave scattering problems and evaluating wave forces acting on the arrangements under consideration, as discussed in Fig. 3. It is also important to mention that the model is valid for any number of compound cylinders although here it is considered only for three configurations as test cases.

1. Wave forces on four compound cylinders arranged as in Fig. 3(a)

Results for the hydrodynamic force on each of the compound cylinders against the non-dimensional wavenumber ka are presented in Fig. 7 for different values of h/a and b/a. In Fig. 7(a), four different values of h/a are considered, and a few numbers of peaks and zero values of force, which occur due to the constructive and destructive interference of the waves, are observed for all the cases. These peaks attain a high rise at a specific value of wavenumber ka, known as a force spike - a well-established phenomenon that occurs due to the trapping of the high amplitude of waves[33,35]. This clearly indicates the waves being scattered from the cylinders, which will be more prominent when we simulate the waves in the time domain in § IV. In this case, only one spike exists in the force acting on the rigid cylinder of each compound cylinder. Further, it is observed that, in the absence of the porous wall around the rigid cylinder, the force acting on the cylinder has multiple numbers of small spikes, as seen in Fig. 2. Hence, it is worth mentioning that covering each of those cylinders with a porous wall would safeguard the entire structure since the force magnitude would reduce to a reasonable extent. Next, keeping the value of h/a constant at 2 and varying the thickness of the porous wall, the force term is plotted in Fig. 7(b). It is noticed that the second force spike begins roughly at $ka = 6.5$ when b/a is 1.5; it changes to $ka = 4.3$ for $b/a = 1.8$; and again shifts to 3.3 for $b/a = 2.0$. It leads to the conclusion that, as the value of b/a rises, two force spikes appear, with the second force spike shifting toward the first as the compound cylinders come closer to each other.

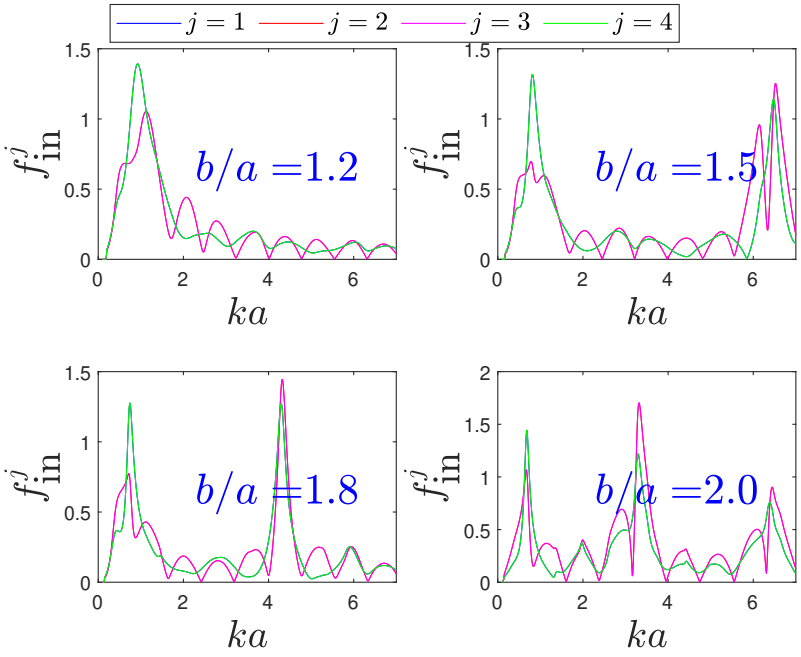

(a)

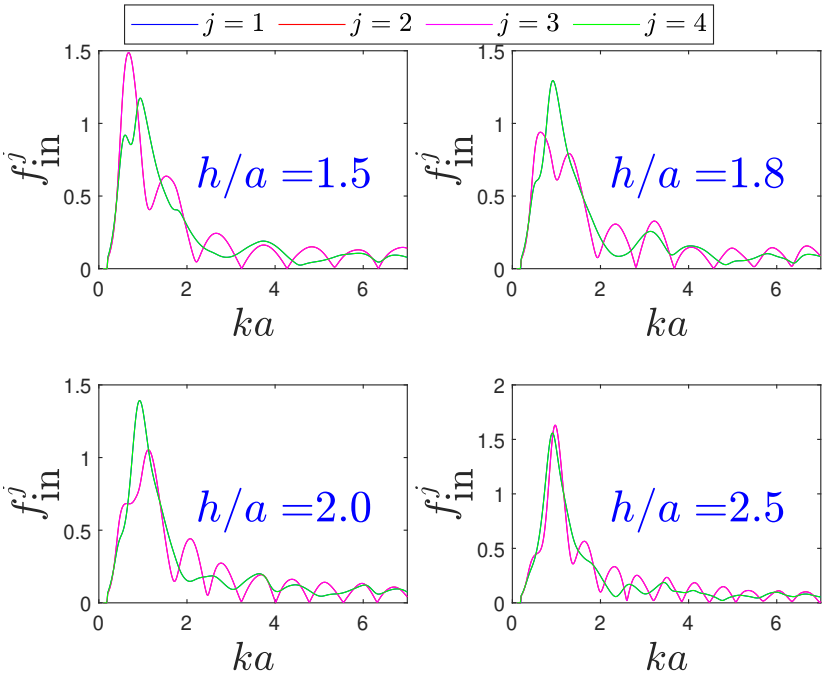

(b)

FIG. 7. Force on the rigid cylinder against non-dimensional wavenumber ka for four compound cylinders with $\beta = 0^\circ$ and $G = 0.1$, (a) different values of h/a with $b/a = 1.25$; (b) different values of b/a with $h/a = 2$

(a) (b)

FIG. 8. Contour plot for (a) maximum value of f_{in}^{1}; (b) corresponding ka with the variation of Re(G) and Im(G) for $N = 4$; $h/a = 2$; $b/a = 1.25$ and $\beta = 0$

It is observed that, by considering $h/a = 2$ and $b/a = 1.25$, one force spike in the graph corresponds to each of the compound cylinders. It is also essential to analyze the effect of G on the force term. Generally, the porous-effect parameter G has the complex form comprising Re(G) and Im(G) which denote the resistance and inertial effect, respectively. Hence, for the first compound cylinder, we show the force spikes and their associated wavenumbers against the variation of Re(G) and Im(G) in Fig. 8. It can be observed from Fig. 8(a) that the force spike magnitude is minimum when Re(G) > Im(G), i.e., when the resistance effect dominates the inertial effect. Also, it is observed from Fig. 8(b) that the force spikes exist for the values of ka $\mathsf{2}$ $(1, 2)$ for the given ranges of Re(G) and Im(G). The same graphical analysis can be carried out for other configurations as well. However, it is not carried out here to avoid repetitions.

It will also be interesting to visualize the free surface elevation at those specific values of G and ka, for which the force spikes attain maximum and minimum values. The free surface plot is presented in Fig. 9 by considering $\mathsf{j}\phi(r, \theta)\mathsf{j}$. In Fig. 9(a), the elevation plot is shown for $G = 0.1 + 0.3\text{i}$, $ka = 1.42$, for which the force spike attains the maximum value of 2.4 as observed from Fig. 8(a). At the given values of the parameters, it can be observed from the graph that the waves of high amplitude get trapped in the vicinity of the compound cylinders and can create resonance in the system. Similarly, the elevation plot is shown in

FIG. 9. Wave elevation for (a) G = 0:1 + 0:3i; ka = 1:42; (b) G = 0:6 + 0:2i; ka = 1:16 for N = 4; = 0 ; h=a = 2 and b=a= 1:25

Fig. 9(b) for $G = 0.6 + 0.2\mathrm{i}$, $ka = 1.16$ where the force spike attains the minimum value of 1.6. Although the waves get localized near the compound cylinder in this case, the wave amplitude is 1.8, which is comparatively less than in the previous case. Hence, the wave impact for four compound cylinders placed in an array gets minimized when the resistance effect of the porous wall is higher than the inertial effect of the shell.

2. Wave forces on five compound cylinders arranged as in Fig. 3(b)

Here, the arrangement consists of five compound cylinders, out of which four lie at the corners of the square of side $2h$ and the other is located at the center of the square. We need to consider $\sqrt{2}h > 2b$, which ensures that the compound cylinders do not overlap. To understand the wave impact on the force acting on the inner cylinder inside each compound cylinder, β is taken as $\pi/4$, and the results are presented in Fig. 10. It is observed from Fig. 10(a) that, for all the compound cylinders, the wave force increases and attains its maximum value at a critical point of ka and then decreases to zero. Also, this maximum value of the force term increases as the gap between the compound cylinders decreases. The effect is more prominent on the third and fifth compound cylinders, whose centers are at $(-h, h)$ and $(0, 0)$, respectively. Next, by fixing $h/a = 3$ and varying b/a, such that $b < h/\sqrt{2}$, we present the graphs for the wave force in Fig. 10(b). It is observed that, with an increase in the thickness of the porous wall, the wave force increases and attains its maximum at more than one point. When $b/a = 2.1$, i.e., when the compound cylinders are

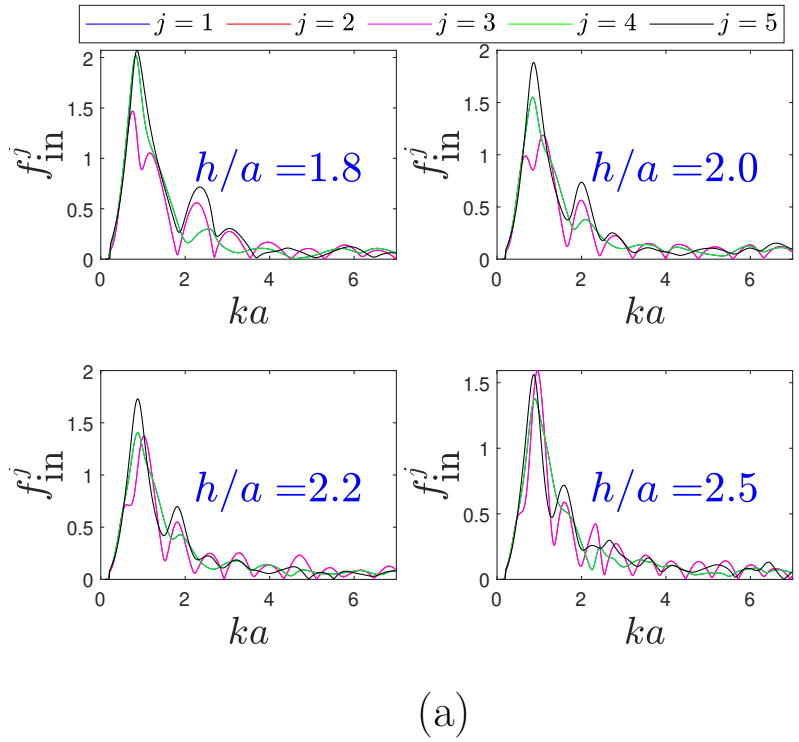

(a)

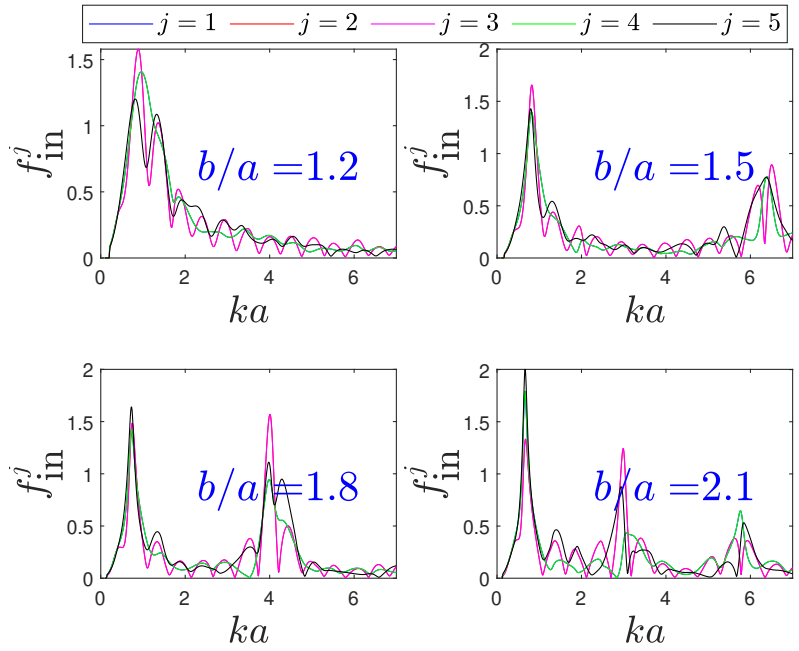

(b)

FIG. 10. Force on the rigid cylinder against non-dimensional wavenumber ka for five compound cylinders with $\beta = 45°$ and $G = 0.1$, (a) different values of h/a with $b/a = 1.25$; (b) different values of b/a with $h/a = 3$

very close to each other, three maxima values of the force occur at $ka = 0.61, 2.99$, and 5.79

for all the compound cylinders.

(a) (b)

FIG. 11. Contour plot for (a) maximum value of f_{in}^5; (b) corresponding ka with the variation of $\text{Re}(G)$ and $\text{Im}(G)$ for $N = 5$; $h/a = 3$; $b/a = 1.25$ and $\beta = 45^\circ$

The effect of the complex porous-effect parameter of the porous wall on the wave force is presented in Fig. 11 for the fifth compound cylinder placed at the origin. For $\text{Re}(G) > 0.3$ and $\text{Im}(G) > 0.6$, the magnitude of the force spike is nearly constant between 1.8 and 2. The value of the force spike is noticeably higher for $\text{Re}(G) < 0.3$, and it reaches a maximum

(a) (b)

FIG. 12. Wave elevation for (a) $G = 0.1 + 0.3\text{i}, ka = 1.6$; (b) $G = 0.6 + 0.2\text{i}, ka = 1.36$ for $N = 5$; $\beta = 45^\circ$; $h/a = 3$ and $b/a = 1.25$

value of 3 at $0.1 + 0.3\text{i}$ (Fig. 11(a)). For any value of G, this force spike exists uniformly at $ka = 1.4$. Very small variation in the value of ka is observed for $\text{Re}(G) < 0.2$ and

$\mathrm{Im}(G) < 0.6$ (Fig. 11(b)). Therefore, based on this plot, we choose two values of G and

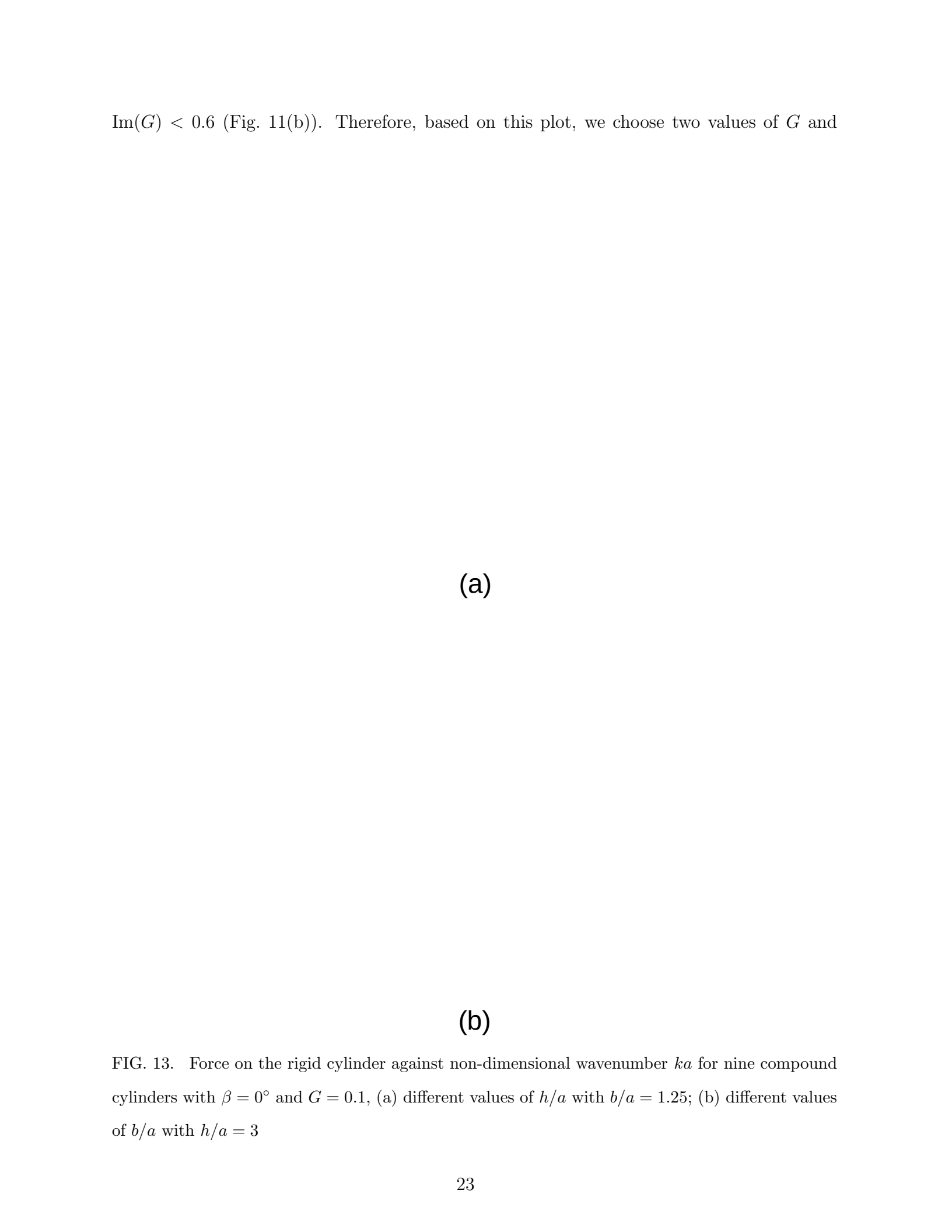

FIG. 13. Force on the rigid cylinder against non-dimensional wavenumber ka for nine compound cylinders with $\beta = 0^\circ$ and $G = 0.1$, (a) different values of h/a with $b/a = 1.25$; (b) different values of b/a with $h/a = 3$

the associated ka such that the minimum and maximum force peaks are at 1.7 and 2.5, respectively. We depict the free surface wave elevation for these two sets of values of G and ka in Fig. 12.

3. Wave forces on nine compound cylinders arranged as in Fig. 3(c)

Here we consider nine compound cylinders, and the numbering of those cylinders is given in Fig. 3(c). For simplicity in the computation, we consider $\beta = 0^\circ$ and hence, due to the symmetry, the force acting on the first and the seventh compound cylinders are the same. Similarly, the other pairs with the same wave forces are the second and the sixth compound cylinders; the third and the fifth compound cylinders. Through the plots shown in Fig. 13(a), it is clear that, as discussed before, one force spike exists for all the values of h/a. It is important to note that the magnitude of this force spike is quite high compared to the other two arrangements of the compound cylinders, possibly due to the presence of more numbers of structures within the given length $2h$ of the square. The same is also reported in the work of Liu et al.[36]. The pattern remains the same as discussed for the variation of thickness of the porous wall, which is visible in Fig. 13(b).

(a) (b)

FIG. 14. Contour plot for (a) maximum value of f_{in}^1; (b) corresponding ka with the variation of Re(G) and Im(G) for $N = 9$; $h/a = 3$; $b/a = 1.25$ and $\beta = 0^\circ$

The contour plot given in Fig. 14 shows the effect of the complex porous-effect parameter

(a) (b)

(c) (d)

FIG. 15. Wave elevation for (a) $\beta = 0°$, (b) $\beta = 30°$, (c) $\beta = 60°$, (d) $\beta = 90°$ with $G = 0.1 + 0.3\text{i}$; $ka = 1.82$; $b/a = 1.25$; $h/a = 3$ and $N = 9$

of the porous wall on the magnitude of wave force spike for the first compound cylinder in order to get an overview of how it affects the wave forces acting on the structure. It is observed here that, for $\text{Im}(G) > \text{Re}(G)$, the magnitude of the force spike increases. The values of ka for which those spikes exist can be obtained from the plot shown in Fig. 14(b). Hence, for plotting the elevation, we consider $G = 0.1 + 0.3\text{i}$; $ka = 1.82$, where the force spike attains the maximum value of 5.0. As observed from Fig. 15, we consider surface plots for four different values of incident angles. The wave localization with high amplitude is observed in each subfigure, with the position changing with a change in the value of the incident angle.

IV. NUMERICAL RESULTS WITH TIME-DEPENDENT FORCING

The wave forces in the previous section correspond to a given frequency. If we consider a simple time-dependent problem, then it will be possible to visualize the motion of the structure and the effect of the force on the structure in the long run, which, otherwise, cannot be achieved by considering only the frequency domain solution. In other words, we have to account for the effect of time on the problem. We achieve this by considering a Gaussian pulse in the frequency domain and utilizing Fourier transform to generate a wave pulse in the time domain. In the dimensionless form, the wavenumber, frequency and time

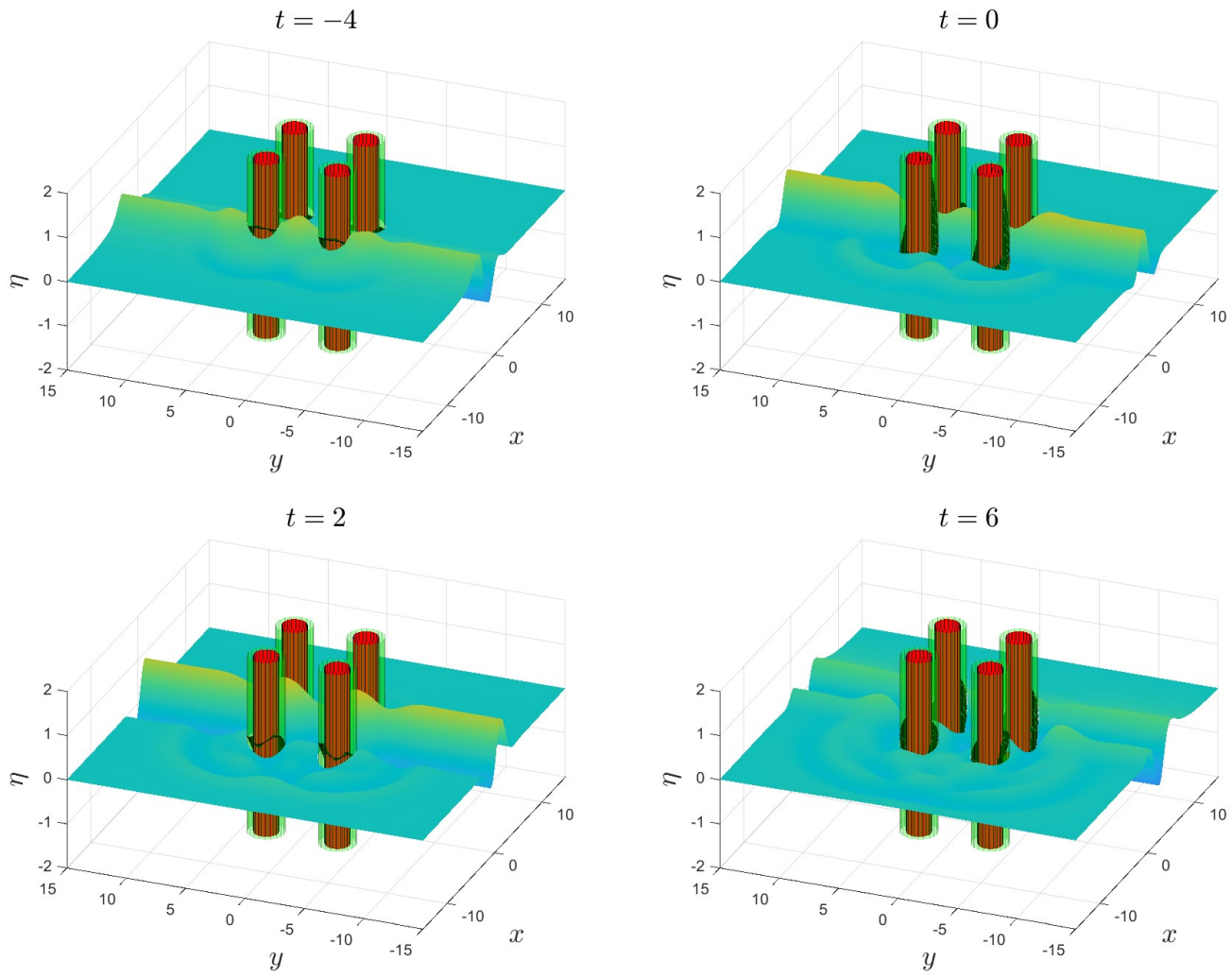

FIG. 16. Wave elevation for different time with $G = 0.1 + 0.3\mathrm{i}$; $k_c = 1$; $\sigma = 1.25$; $\beta = 0°$. The full animation can be found in Movie-1.

are denoted by $\hat{k} = ka$, $\hat{\omega} = \omega\sqrt{a/g}$, $\hat{t} = t\sqrt{g/a}$ and $\hat{\eta} = \eta/A$, respectively. However, the

hat is dropped hereafter without any loss of generality, and the time domain displacement of the structure can be expressed as

$$\eta(x,y,t) = \mathrm{Re}\left[\int_0^\infty f(k)\tilde{\eta}(x,y,0)e^{\mathrm{i}\omega t}dk\right], \tag{35}$$

where $f(k) = \frac{\sqrt{\sigma}}{\pi}\exp(\sigma(k-k_0)^2)$, with scaling factor σ and central wavenumber k_0, and $\tilde{\eta}(x,y,0)$ represents the wave amplitude in the frequency domain.

At this juncture, we aim to carry out a time domain simulation to visualize the wave transition and the resonant behaviour of the system for a given set of parameters chosen from the previous section.

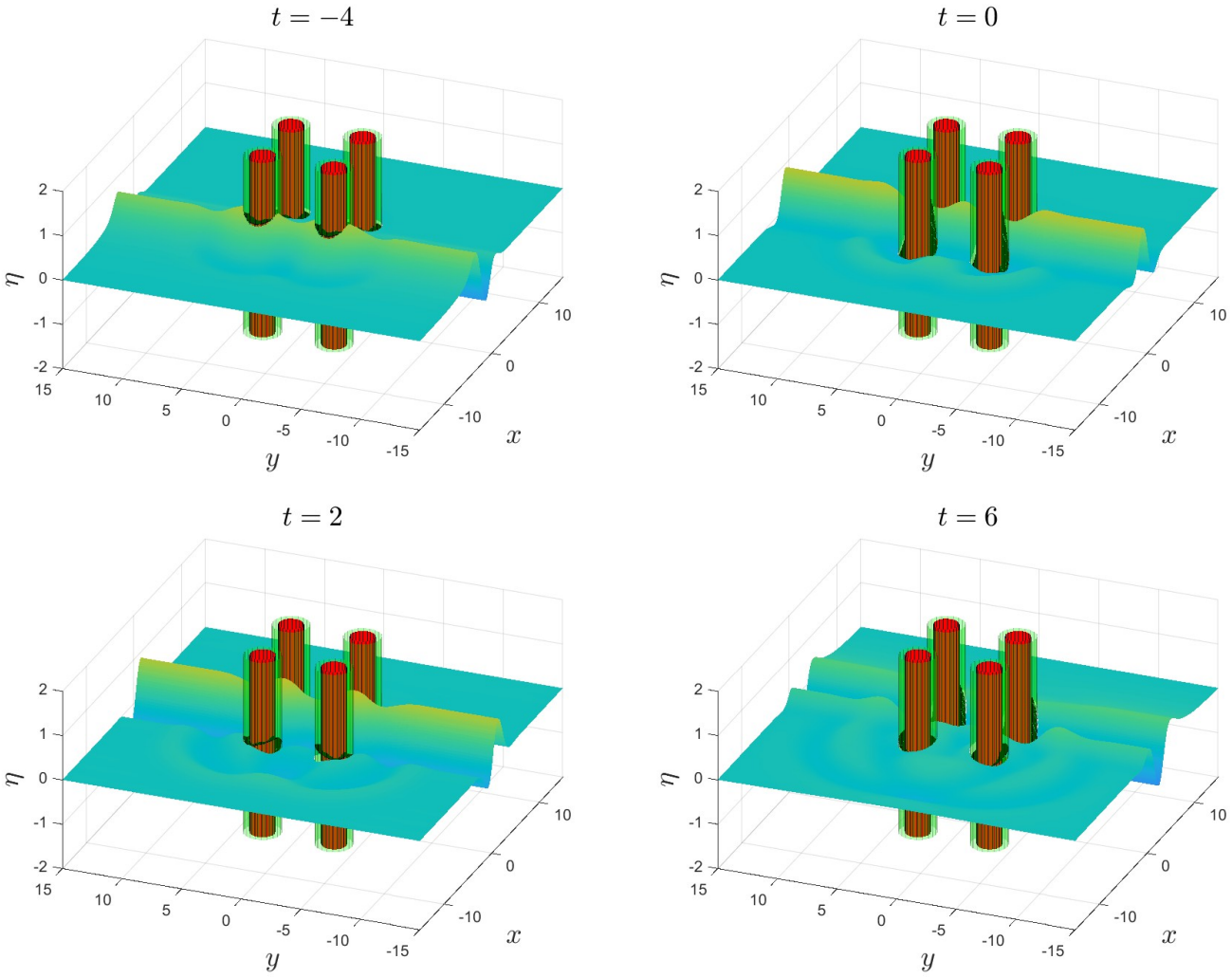

FIG. 17. Wave elevation for different time with $G = 0.6 + 0.2\mathrm{i}$; $k_c = 1$; $\sigma = 1.25$; $\beta = 0°$. The full animation can be found in Movie-2.

We may recall that, for a four compound cylinder configuration, the force spike reaches its

maximum for $G = 0.1+0.3\text{i}$ and it is minimum for $G = 0.6+0.2\text{i}$ (Fig. 9). As a result, for the time domain simulation, we take into account these two G values and simulate the surface wave profile in the near-field by displaying two movies, Movie-1 and Movie-2, with a Gaussian impulse. Figures 16 and 17, respectively, show a few snapshots of the same for $t = -4, 0, 2$ and 6. Here, $t < 0$ represents the solution when the Gaussian beam approaches the system, and the peak of the beam aligns with the center of the system at $t = 0$. It is straightforward to see how the wave pulse enters the system, impacts it, and disperses (especially from the movies). Relatively higher amplitude of surface profile is observed within the structures. The regular arrangement of the cylinders leads to resonant scattering, which can lead to near-trapping. As with any multiple scattering, there will be occurrence of constructive and

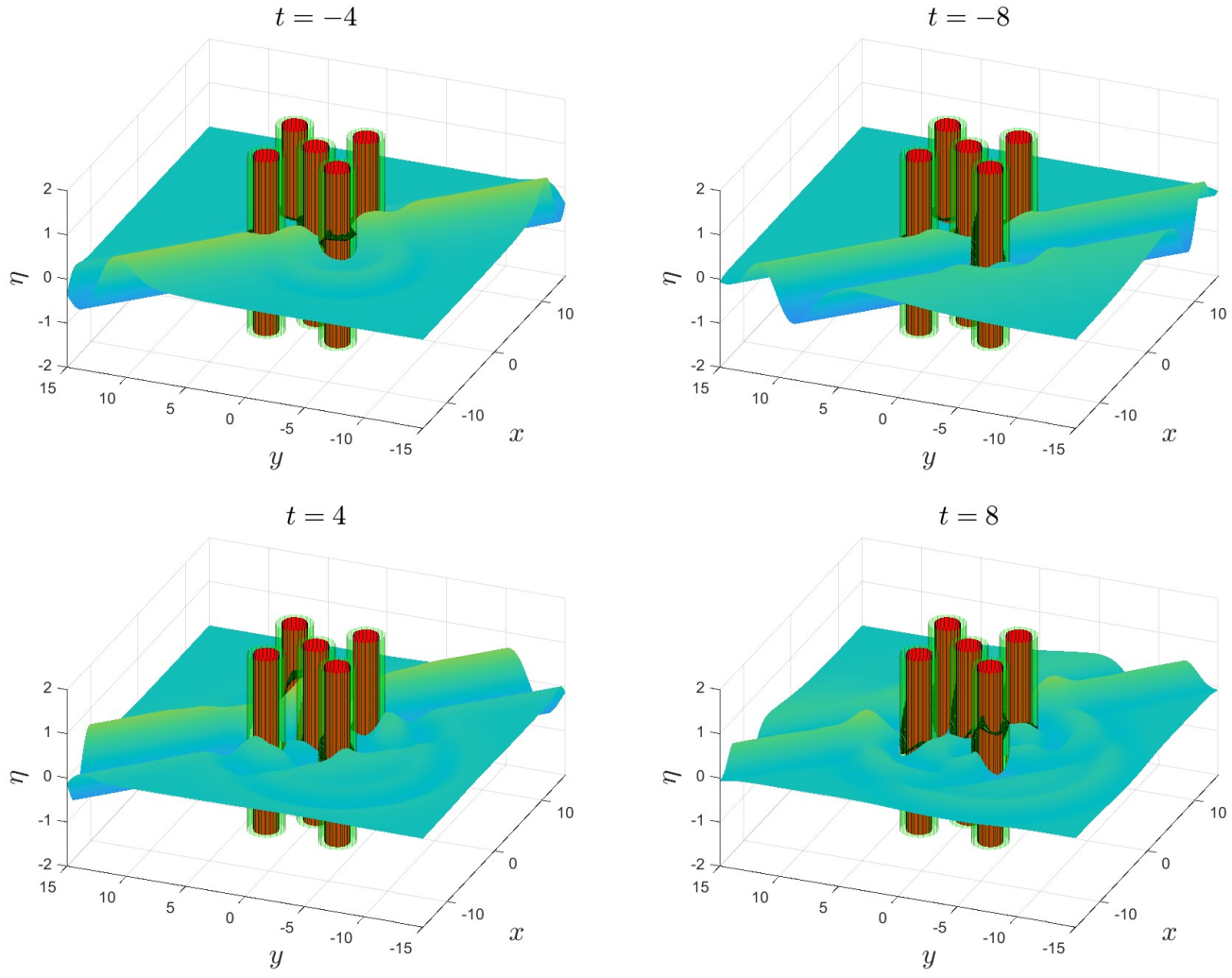

FIG. 18. Wave elevation for different time with $G = 0.1 + 0.3\text{i}$; $k_c = 1$; $\sigma = 1$; $\beta = 45°$. The full animation can be found in Movie-3.

destructive interference, which is made stronger by the regular arrangement of the cylinders. The simulation illustrates how the incident wave is scattered, resulting in a roughly circular outgoing wave. It also shows the effects of multiple scattering and the resonance caused by the multiple cylinders. These features will also be observed in the subsequent simulations when other cylinder configurations, porous-effect parameters, and incident wave angles are used.

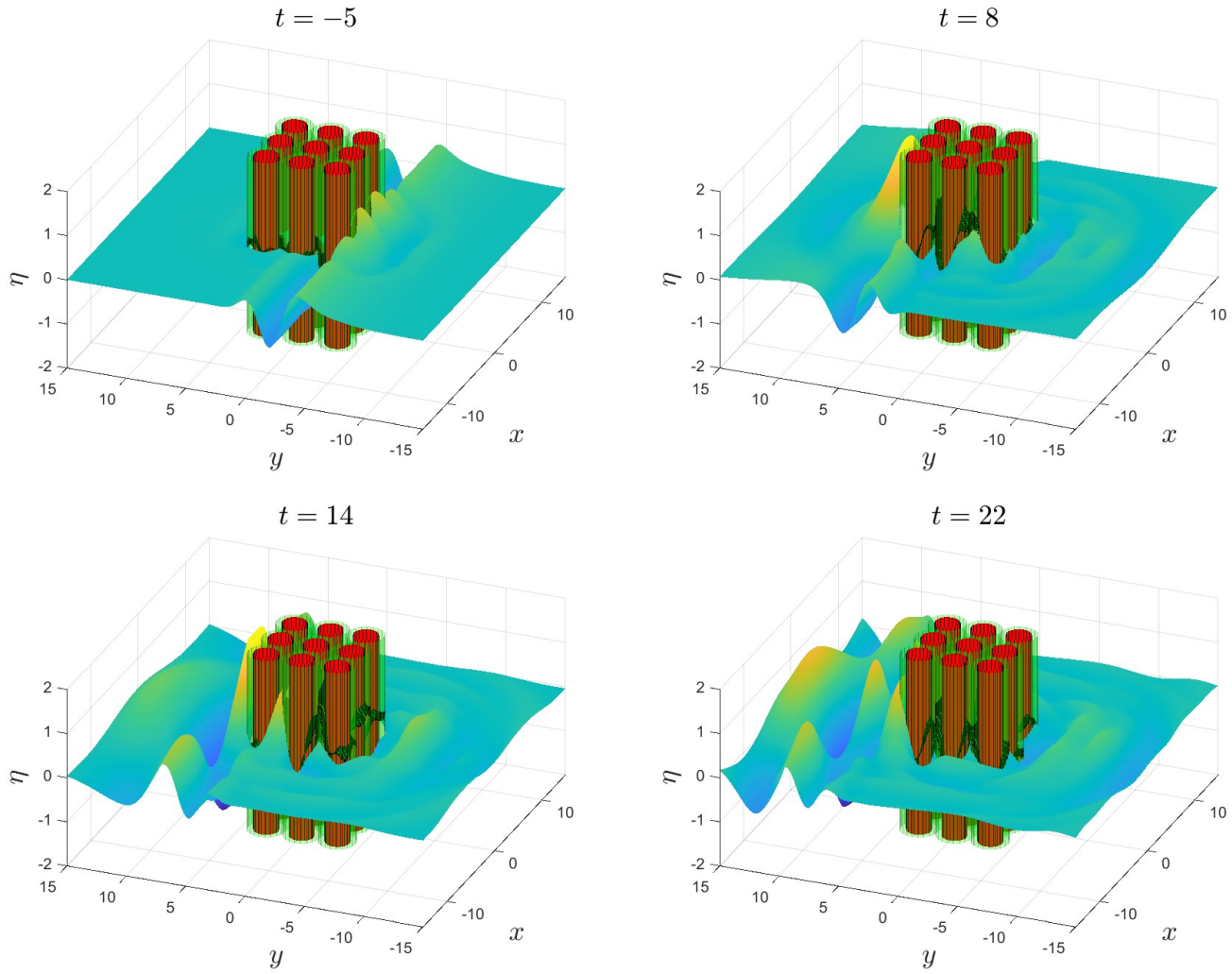

FIG. 19. Wave elevation for different time with $G = 0.1 + 0.3\mathrm{i}$; $k_c = 1$; $\sigma = 1$; $\beta = 90°$. The full animation can be found in Movie-4.

Five compound cylinders in Movie-3 can be seen in an undisturbed position prior to the arrival of the impulse at an angle of 45°. The beam strikes the structure gradually, scattering the wave around it. Even after the wave impulse exits the area under examination, the resonant behaviour is still visible in the space between the compound cylinders. Figure 18

shows a few images for the same. The same behaviour is also observed in the case of nine compound cylinders which is shown in Movie-4 for an incident angle of 90°, and the corresponding snapshots are shown in Fig. 19. The most striking feature is the comparatively higher amplitude of the waves in the transmitted region of the compound cylinder.

V. CONCLUSION

A variety of marine structures are known to consist of several circular-shaped vertical cylinders. It is also a well-established fact that a porous wall acts as a good wave absorber around a rigid cylinder in protecting it from long-term wave impact. In this direction, to examine the long-term effects of wave interaction with such a structure, we consider the model proposed by Sankarbabu et al.[17] and perform the time-dependent study. Following the same technique as adopted in their work, we first presented the analytical solution in the frequency domain. Apart from the calculation of the hydrodynamic forces, we have also provided the derivation of the wave power dissipation which has not been studied earlier for such a set-up. For validation of the considered model, four vertical cylinders, positioned on the circle of a specified radius, were considered without accounting for the porous walls. Excellent agreement of the results was obtained with the works of Teng et al.[32] and Evans and Porter[33]. Upon validation, three different configurations of the compound cylinders were considered for carrying out numerical experiments of the wave impact: (i) four compound cylinders with their centers located at four corners of a square, (ii) same configuration as above with one extra compound cylinder at the center of the square $(4 + 1)$ and (iii) eight compound cylinders (putting one extra cylinder in each of the sides of the square) with one extra cylinder at the center of the square $(8 + 1)$. For all the configurations, the effect of complex porous-effect parameter on the hydrodynamic forces and the wave run-up was examined. For the proposed model, only the impact of the real part of G was considered in the numerical study.

The precise conclusions drawn in the frequency domain for all the configurations are as follows:

1. There always exists a critical wavenumber at which the force spike occurs for all the compound cylinders. This could be due to the wave scattering between the compound cylinders.

2. In addition to one force spike, another one also shows its existence with the increase in the separation distance between the porous wall and the rigid cylinder.

3. The magnitude of the force spike is less when the resistance part of the porous-e ect parameter dominates the inertial e ect and more when the inertial e ect suppresses the resistance e ect.

Locating those critical points of the wavenumber with its suitable geometrical con gurations, di erent wave elevation plots are also shown for di erent values of incident angle. After that, we analyzed how this a ects the time-dependent solution by considering the system's response to a Gaussian impulse. Di erent movie plots were shared for better visualization of the solution and to understand the long-term e ect of wave scattering on the structure.

DECLARATIONS

Acknowledgments

The corresponding author is grateful to Science and Engineering Research Board (SERB) of the Department of Science and Technology (DST), Govt. India for necessary funding, Indian Institute of Technology Guwahati for allowing her to execute her research by hosting her for certain duration, and her employer Vellore Institute of Technology Vellore for allowing her to execute her research and also for granting her the required leave to carry out research with her mentor (rst author) at Indian Institute of Technology Guwahati. All authors thank the learned Reviewers for making meaningful observations and comments which immensely helped in producing an e ective revision. The Handling Associate Editor Dr. Rossana Pasquino is profusely thanked for allowing a revision.

Funding

This work is funded by Science and Engineering Research Board (SERB) of the Department of Science and Technology (DST), Govt. of India under TARE scheme through the grant TAR/2021/000177 awarded to Sunanda Saha.

Con ict of interest

The authors of the article declare not to have con ict of interests that may interfere in the impartiality of the scienti c work.

Availability of data and materials

Some or all data, models, or code that support the ndings of this study are available from the corresponding author upon reasonable request. There is no data that is used for this work. MATLAB codes are available with the authors which, if required, can be obtained from the corresponding author.

REFERENCES

[1]B. H. Spring and P. L. Monkmeyer, \Interaction of plane waves with vertical cylinders," In: Proceedings 14th International Coastal Engineering Conference , 1828{47 (1974).

[2]M. J. Simon, \Multiple scattering in arrays of axisymmetric wave-energy devices. part 1. a matrix method using a plane-wave approximation," J. Fluid Mech120, 1{25 (1982).

[3]P. McIver and D. V. Evans, \Approximation of wave forces on cylinder arrays," J. Fluid Mech. 6, 101{7 (1984).

[4]H. Kagemoto and D. K. P. Yue, \Interactions among multiple three-dimensional bodies in water waves: An exact algebraic method," J. Fluid Mech166, 189{209 (1986).

[5]C. M. Linton and D. Evans, \The interaction of waves with arrays of vertical circular cylinders," J. Fluid Mech. 215, 549{569 (1990).

[6]K. H. Wang and X. Ren, \Wave interaction with a concentric porous cylinder system," Ocean Eng.21(4) , 343{360 (1994).

[7]M. K. M. Darwiche, A. N. Williams, and K. H. Wang, \Wave interaction with semi-porous cylindrical breakwater," J. Waterway, Port, Coastal, Ocean Eng120, 382{403 (1994).

[8]M. Faltas, \On oblique waves forcing by a porous cylindrical wall," Int. J. Math. Math. Sci. 19, 351362 (1996).

[9]A. N. Williams and L. Li, \Wave interaction with a semi-porous cylindrical breakwater mounted on a storage tank," Ocean Eng25, 195{219 (1998).

[10]G. Govare, R. Silva, and J. A. Maza, "Wave kinematics around a protected cylindrical impermeable pile," Coastal Structures, 99, ASCE, Santander, Spain, Balkema, Rotterdam , 151–8 (1999).

[11]A. Chanda and A. Sarkar, "Structural performance of a submerged bottom-mounted compound porous cylinder on the water wave interaction in the presence of a porous sea-bed," Phys Fluid **34**, 092113 (2022).

[12]J. Liu, G. Lin, and J. Li, "Short-crested waves interaction with a concentric cylindrical structure with double-layered perforated walls," Ocean Eng. **40**, 76–90 (2012).

[13]K. Vijayalakshmi, R. Sundaravadivelu, K. Murali, and S. Neelamani, "Hydrodynamics of a concentric twin perforated circular cylinder system," J. Waterway, Port, Coastal, Ocean Eng. **134 (3)**, 166–177 (2008).

[14]Z. Zhai, S. Zheng, and D. Wan, "Interaction between solitary waves and a combined structure of two concentric asymmetric porous arc walls," Phys. Fluids **34**, 042103 (2022).

[15]A. N. Williams and W. Li, "Water wave interaction with an array of bottom-mounted surface-piercing porous cylinders," Ocean Eng. **27**, 841–66 (2000).

[16]O. Umnova, K. Attenborough, and C. M. Linton, "Effects of porous covering on sound attenuation by periodic arrays of cylinders," Journal of the Acoustical Society of America **119**, 278–84 (2006).

[17]K. Sankarbabu, S. A. Sannasiraj, and V. I. Sundar, "Interaction of regular waves with a group of dual porous circular cylinders," Appl Ocean Res **29**, 180–90 (2007).

[18]M. S. Park, Y. J. Jeong, and Y. J. You, "Water wave interaction by dual cylindrical cylinders with partial porous area," International Journal of Engineering and Technology **9** (2017).

[19]C. Wang and Z. Y. Tay, "Very large floating structures: applications, research and development," Procedia Eng. **14**, 62–72 (2017).

[20]W. Nugroho, K. Wang, R. Hosking, and F. Milinazzo, "Time-dependent response of a floating flexible plate to an impulsively started steadily moving load," J. Fluid Mech. **381**, 337–355 (1999).

[21]K. Wang, R. Hosking, and F. Milinazzo, "Time-dependent response of a floating viscoelastic plate to an impulsively started moving load," J. Fluid Mech. **521**, 295–317 (1999).

[22]M. Meylan and I. Sturova, "Time-dependent motion of a two-dimensional floating elastic plate," J. Fluid. Struct. **25**, 445–460 (2009).

[23]M. Meylan, "The time-dependent vibration of forced floating elastic plates by eigenfunction matching in two and three dimensions," Wave Motion **88**, 21–33 (2019).

[24]M. Meylan, "Time-dependent motion of a floating circular elastic plate," Fluids **6(1)**, 29 (13 pages) (2021).

[25]M. H. Meylan and R. E. Taylor, "Time-dependent water-wave scattering by arrays of cylinders and the approximation of near trapping," J. Fluid Mech. **631**, 103–125 (2009).

[26]S. A. Selvan, R. Gayathri, H. Behera, and M. H. Meylan, "Hydrodynamic performance and energy absorption of multiple spherical absorbers along a straight coast," Phys Fluid **33**, 037119 (2021).

[27]S. Saha, S. N. Bora, and S. Das, "Time-dependent water wave scattering by bottom-mounted porous compound cylinder fitted with an annular porous lid," Waves Random Complex Media , doi.org/10.1080/17455030.2023.2166150 (2023).

[28]X. Yu, "Diffraction of water waves by porous breakwaters," J. Waterway, Port, Coastal, Ocean Eng. **121**, 275–282 (1995).

[29]F. Zhaoa, T. Kinoshit, W. Bao, R. Wana, Z. Liang, and L. Huang, "Hydrodynamics identities and wave-drift force of a porous body," Appl. Ocean Res. **33**, 169–177 (2011).

[30]G. N. Watson, "A treatise on the theory of bessel functions," Cambridge University Press (1922).

[31]S. Zheng, S. Michele, H. Liang, M. H. Meylan, and D. Greaves, "Wave power extraction from a floating elastic disk-shaped wave energy converter," J. Fluid Mech. **948** (2022).

[32]B. Teng, L. Han, and Y. Li, "Wave diffraction from a vertical cylinder with two uniform columns and porous outer wall," China Ocean Eng. **14(3)**, 297–306 (2000).

[33]D. Evans and R. Porter, "Near-trapping of waves by circular arrays of vertical cylinders," Appl. Ocean Res. **19**, 83–99 (1997).

[34]M. H. Meylan, L. G. Bennetts, and M. A. Peter, "Water-wave scattering and energy dissipation by a floating porous elastic plate in three dimensions," Wave Motion **70**, 240–250 (2017).

[35]D. Evans and R. Porter, "Trapped modes about multiple cylinders in a channel," J. Fluid Mech. **339**, 331–356 (1997).

[36]Y. Liu, S. Zheng, H. Liang, and P. Cong, "Wave interaction and energy absorption from arrays of complex-shaped point absorbers," Phys. Fluids **34**, 097107 (2022).